

# Mechanical response of flexible pavements enhanced with geogrid-reinforced asphalt overlays

N. S. Correia<sup>1</sup> and J. G. Zornberg<sup>2</sup>

<sup>1</sup>Postdoctoral Researcher, University of Sao Paulo at Sao Carlos, Department of Geotechnical Engineering, 13566-536, Sao Carlos, SP, Brazil, Telephone: +55 16 3373 9505; Telefax: +55 16 3373 9509; E-mail: nati.correia@gmail.com (corresponding author)

<sup>2</sup>Professor, The University of Texas at Austin, Civil Engineering Department, University Station C1792 Austin, TX 78712-0280, USA, Telephone: +1 303 492 0492; Telefax: +1 512 471-6548; E-mail: zornberg@mail.utexas.edu

Received 25 May 2015, revised 1 September 2015, accepted 19 September 2015, published 9 December 2015

**ABSTRACT:** The use of geosynthetic reinforcements placed underneath asphalt overlays, which has been typically used to minimise problems associated with reflective cracking, is evaluated in this study as an approach to improve pavement structural capacity. Whereas geosynthetics have been used to increase the pavement structural performance when used to reinforce the base aggregate, as reported in numerous laboratory and evaluations experiments, such improvement has not been evaluated for the case of geosynthetics within asphalt layers. Accordingly, this paper presents the results of large model tests involving both reinforced and unreinforced hot mix asphalt overlays. Cyclic wheel loads were applied using an accelerated pavement test facility that was specifically developed for this research. A number of pavement sections were constructed using a polyvinyl alcohol geogrid as reinforcement inclusions. The results show a considerable increase in pavements structural performance, as quantified by reduction of strains in the asphalt concrete layers, in the vertical stresses within the pavement layers and in the resilient displacements at the wearing surface. The use of geogrid reinforcements was also found to lead to reduce rutting and permanent lateral movements in the surface layer. Overall, the use of geogrids within asphalt overlays was found to act as a reinforcement element that provide enhanced structural capacity to flexible pavements.

**KEYWORDS:** Geosynthetics, Asphalt overlay, Geogrid, Pavement, Reinforcement

**REFERENCE:** Correia, N. S. and Zornberg, J. G. (2016). Mechanical response of flexible pavements enhanced with geogrid-reinforced asphalt overlays. *Geosynthetics International*, 23, No. 3, 183–193. [<http://dx.doi.org/10.1680/jgein.15.00041>]

## 1. INTRODUCTION

Geosynthetics have been used to improve the pavement structural performance when used as reinforcements within the aggregate base layer, as reported in numerous laboratory and field evaluations (Perkins 1999; Zornberg and Gupta 2010; Tang *et al.* 2015; Wu *et al.* 2015). However, geosynthetic reinforcements placed underneath asphalt overlays have been used almost exclusively to reduce the development of reflective cracking into asphalt overlays, without accounting for their capability to potential increase the pavement structural capacity. This study evaluates the potential use of geosynthetic-reinforced asphalt overlays to enhance the overall pavement structural capacity. This approach is expected to lead to significant advances in pavement rehabilitation by extending the life of roadways, consequently reducing maintenance costs.

The use of geosynthetics to improve the service life of pavements in asphalt overlays (either new asphalt layers or

localised repairs) has increased markedly in recent years. Field evidence and theoretical studies have indicated that the service life of flexible pavements can be extended by installing nonwoven geotextiles or geogrids between the existing layer and the new asphalt overlays due to the ability of the geosynthetic to minimise the development of reflective cracks (Lytton 1989; Austin and Gilchrist 1996; Prieto *et al.* 2007; Khodaii *et al.* 2009; Virgili *et al.* 2009; Yu *et al.* 2013; Fallah and Khodaii 2015; Gonzalez-Torre *et al.* 2015). However, a more limited number of studies has been initiated to assess the use of geosynthetics in asphalt overlays to improve the mechanical performance of pavements, such as control of permanent displacements. While in many of these studies, the main focus has been the control of reflective cracks, the reported evidence of improved pavement capacity are summarised next.

Brown *et al.* (1985) reported that polypropylene geogrids placed underneath asphalt layers resulted in a decrease in rutting ranging from 20 to 58%. Austin and Gilchrist (1996) reported that the use of geogrid in

an asphalt concrete layer contributed to reduce lateral flow and, hence, the development of permanent deformations. Comparisons between the results obtained in unreinforced and reinforced slabs resulted in rutting reductions as great as 70%. An experimental study conducted by Laurinavičius and Oginskas (2006) involving the use of geogrids in asphalt overlays reported reductions in rutting depth of over 50%. Bühler (2007) reported results of a field study in which geogrids were found to reduce rutting depths by 40% in relation to the results obtained in a control section. Using a MMLS3 load simulator, Solaimanian (2013) reported a reduction of up to 85% in the permanent deformations of a pavement model constructed using geogrids between a concrete slab and an asphalt layer. Canestrari *et al.* (2015) conducted flexural beam tests in order to investigate the impact of geogrid reinforcements placed at the interface between two asphalt layers. The use of geogrids resulted in decreased permanent deformations in relation to unreinforced specimens. More recently, Mounes *et al.* (2015) evaluated permanent deformations in geogrid-reinforced asphalt concrete using dynamic creep tests, and concluded that both the mechanical properties and the opening size of the geogrid have a significant importance in controlling permanent deformations. Pasquini and Bocci (2014) conducted interface shear tests on double-layered reinforced samples focusing on interlayer shear resistance and concluded that improved mechanical properties were achieved, although they cautioned about reductions in interlayer bonding (Zamora-Barraza *et al.* 2010; Ferrotti *et al.* 2012).

A valuable approach to quantify the effectiveness of geosynthetic reinforcements to improve the pavement structural performance involves testing full-scale instrumented pavement sections (Perkins 1999). However, most of the current knowledge regarding the use of geosynthetics in a reinforcement function in a pavement have involved the reinforcement of unbound aggregates (Perkins and Ismeik 1997; Holtz *et al.* 1998; USACOE 2003). While these studies are relevant, the mechanisms identified for geosynthetic-reinforced base layers cannot be directly applied to understand the behaviour of geosynthetics in reinforced asphalt layers. Only a limited number of studies have been specifically conducted to investigate the improvement in the behaviour of reinforced asphalt overlays in full-scale instrumented pavement sections, as detailed next.

Siriwardane *et al.* (2010) reported the results of instrumented pavement sections (with and without fibreglass geogrids within the asphalt layer) as a part of a large-scale pavement study. The inclusion of geogrids was found to lead to a decrease in vertical displacements of approximately 38%, as well as a reduction in vertical stresses in the underlying layers. Graziani *et al.* (2014) reported the results of a study on the structural response of geogrid-reinforced asphalt overlays, in which they focused on monitoring the strains within the asphalt layer. The results showed an overall reduction of 65% peak tensile strains in the reinforced section with respect to the unreinforced section.

There are clear opportunities to capitalise on the potential structural improvement that may be realised when using geosynthetic-reinforced asphalt overlays. Accordingly, the objective of this research was to gain understanding on the reinforcement benefits of using geogrids within asphalt overlays, with a focus on the improvements on the pavement performance. An accelerated pavement testing facility was designed and constructed specifically for this study. The investigation involved large-scale laboratory instrumented pavement models, which were loaded using a rolling wheel simulating a truck wheel load.

## 2. TEST FACILITY AND SCOPE OF THE EXPERIMENTAL PROGRAMME

### 2.1. Wheel tracking facility

The large-scale pavement models constructed as part of this study were loaded using a rolling wheel system to simulate the load of a truck wheel. The wheel tracking apparatus was installed in a large steel testing box with internal dimensions of 1.8 m (height), 1.6 m (width) and 1.8 m (length). The testing facility involved steel-reinforced walls that had been designed to withstand high lateral soil stresses with minimum lateral deformations. Accordingly, plane strain conditions were considered to be representative for the models. The stiffness of the structure was enhanced by a reaction beam fixed to the walls of the box, which acted as part of the load transfer system. To properly represent the structural section of a flexible pavement, the testing box was used to house three pavement structural layers: subgrade soil, aggregate granular base, and hot mix asphalt. Figure 1 illustrates the wheel tracking facility.

The wheel load is controlled by a hydraulic jack, which has been designed to apply unidirectional loads of up to 2 t. A hydraulic motor was used to control the movement of the entire system (wheel, jack, load cell). The test wheel (one-tyre configuration) travels at a speed of 3.6 km/h in contact with the tracking length of 1.0 m. The wheel

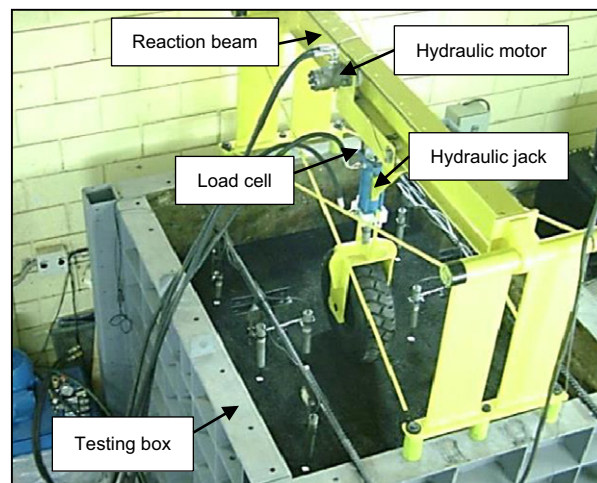


Figure 1. View of the accelerated pavement testing facility

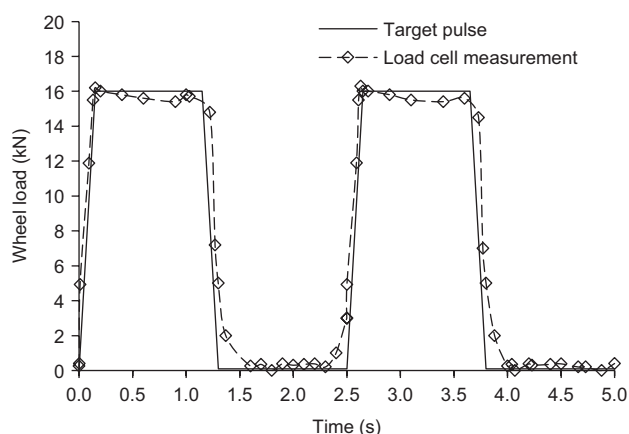


Figure 2. Target wheel load pulse and actually applied load

involves a rubber tyre characterised by a diameter of 546 mm and a width of 154 mm. The tyre pressure was set at 700 kPa. Additional details about the main characteristics of the accelerated pavement test facility are described in Correia (2014).

An in-house software program for data acquisition was developed to control the load-time history of the wheel (cyclic moving load mode). The data acquisition was also used to collect data from the instrument devices installed within the pavement models. The software was programmed to induce the load and wheel pressure pulse shown in Figure 2. The wheel load pulse involves a linear load that increases from 0 to 16 kN over 0.1 s, followed by a period of 1.0 s during which the load is held constant. The load is subsequently reduced to zero over a 0.1 s period. The final period involves a 1.2 s period under zero load before the subsequent load cycle is applied. The various loading stages add up to a total load cycle corresponding to 2.4 s. The output from the load cell for a typical load cycle application is also shown in Figure 2. The results in the figure show a very good match between the target loads and actual applied loads. Each test was conducted until reaching a total of  $10^5$  load cycles.

## 2.2. Pavement materials and layer properties

The geogrid-reinforced and unreinforced asphalt layers were constructed over a dense uniform aggregate base, which was constructed over a soft subgrade. The subgrade soil was classified as MH and A-7-5 according to the USCS (ASTM D 2487-11) and AASHTO (AASHTO M 145 1999) classification systems, respectively. The maximum dry density of subgrade, as determined by Standard Proctor tests was  $14.9 \text{ kN/m}^2$  at an optimum water content of 28.8%. The target dry density and water content were set as  $14.7 \text{ kN/m}^2$  and 30.8% (2% above optimum), resulting in a weak subgrade condition characterised by a California bearing ratio of 4.5%. The bulk density and moisture content of the soil were measured during placement of every 250 mm in elevation. The 1 m thick subgrade layer was compacted in the testing box in 50 mm-thick lifts using manual procedures involving a drop hammer.

The aggregate used as base material classifies as GP and A-1-a according to the USCS (ASTM D 2487-11) and AASHTO (AASHTO M 145) soil classification systems, respectively. The aggregate material was characterised by a maximum dry density of  $24 \text{ kN/m}^3$  and an optimum moisture content of 6.5% based on Standard Proctor tests. Compactions of the base layer were conducted in 100 mm-thick lifts using a vibratory plate. The thickness of the base course layer ranged from 100 to 200 mm, depending on the pavement model, and it was compacted to a target relative compaction of 99% based on Standard Proctor tests.

The hot mixed asphalt (HMA) concrete was a 9.5 mm (3/8") dense-fine-graded mixture with a binder content of 5.4% (Bitumen Penetration Grade 30/45), indicated for all traffic conditions (FHWA and NAPA 2001). The HMA layer was compacted in a single lift of 50 mm using a vibratory plate. For the first stage of tests, the pavement models were composed of a soft subgrade soil, an unbound aggregate base and a HMA layer.

The second stage of tests involved asphalt resurfaced sections. A geogrid that had been specifically manufactured for asphalt application was selected as the reinforcement material (Hatelit XP 50). The geogrid was manufactured using high-modulus polyvinyl alcohol ribs to form a biaxial product with quadrangular apertures. A lightweight polypropylene nonwoven geotextile was attached on one side of the geogrid to facilitate the installation and to allow a continuous bonding to the HMA layer during installation. Index tests were conducted to characterise this reinforcement product (Correia 2014), with results presented in Table 1.

For reinforced sections, the geogrid was cut into the dimensions of the box area and subsequently placed over the previously tested asphalt surface with the geotextile fabric facing down. The machine direction of the geogrid was installed parallel to the wheel tracking path. Previous to the geogrid installation, the asphalt surface had been levelled using HMA concrete. A tack coat rate of cationic rapid setting emulsion ( $0.6 \text{ l/m}^2$  residual) was sprayed in one application (DNER P00/043 2006). Figure 3 illustrates the geogrid installation.

After to the geogrid installation, a new HMA overlay was compacted using the same asphalt concrete material and conditions adopted for construction of the previous asphalt layer. The thickness of the asphalt overlay was

Table 1. Properties of geogrid reinforcement used in this research

Characteristic	Geogrid
Polymer	Polyvinyl alcohol
Aperture size (mm × mm)	40 × 40
Tensile strength (kN/m)	
Machine direction (mm)	50
Cross machine direction (mm)	50
Secant stiffness at 2% strain (kN/m)	890
Elongation at break (%)	5.6

Results obtained using ASTM D6637-11 test method.

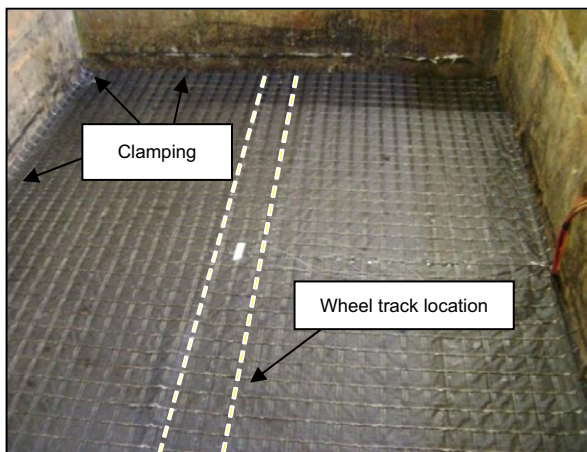


Figure 3. View of the geogrid installation within the testing box

60 mm. The same procedure was used for construction of both reinforced and unreinforced sections.

**2.3. Instrumentation and scope of the testing programme**

An instrumentation programme was designed to monitor the pavement sections during traffic loading in order to quantify the mechanical response of the pavement materials. The instrumentation involved sensors suitable to measure surface vertical displacements, stresses and strains in the asphalt layers, as well as stresses in the base

course and subgrade layers. The data acquisition system used in this study was configured to record information on the entire time history in order to capture the full response of the models under application of the load cycles (Figure 2). All pavement sections were constructed using a similar instrumentation layout. Figure 4 presents the cross-section view of pavement layers and location of the instrumentation devices.

Pressure transducers were used to monitor vertical stresses within the pavement layers. The sensors were installed: (1) at the interface between the old and new asphalt layers, (2) at the interface between the base course and asphalt layer (1 MPa range), (3) in the middle of the base course (500 kPa range) and (4) at the top of the subgrade (200 kPa range). H-type asphalt strain gauges (ASG) were used to measure the asphalt concrete strains at the interface between reinforced and unreinforced asphalt layers. The ASG has a physical range of  $\pm 2000 \mu\epsilon$ . The procedures described by Timm *et al.* (2004) and Graziani *et al.* (2014) were adopted to minimise possible damage to these sensors induced by aggregate particles.

A total of eight linear position transducers (LPT) were used to monitor surface deformation in the transverse direction to the wheel path. The sensors were placed on both sides at four different locations, as follows (distances measured from the wheel load centreline): 240, 390, 540 and 690 mm. Figure 5 illustrates a plan view of

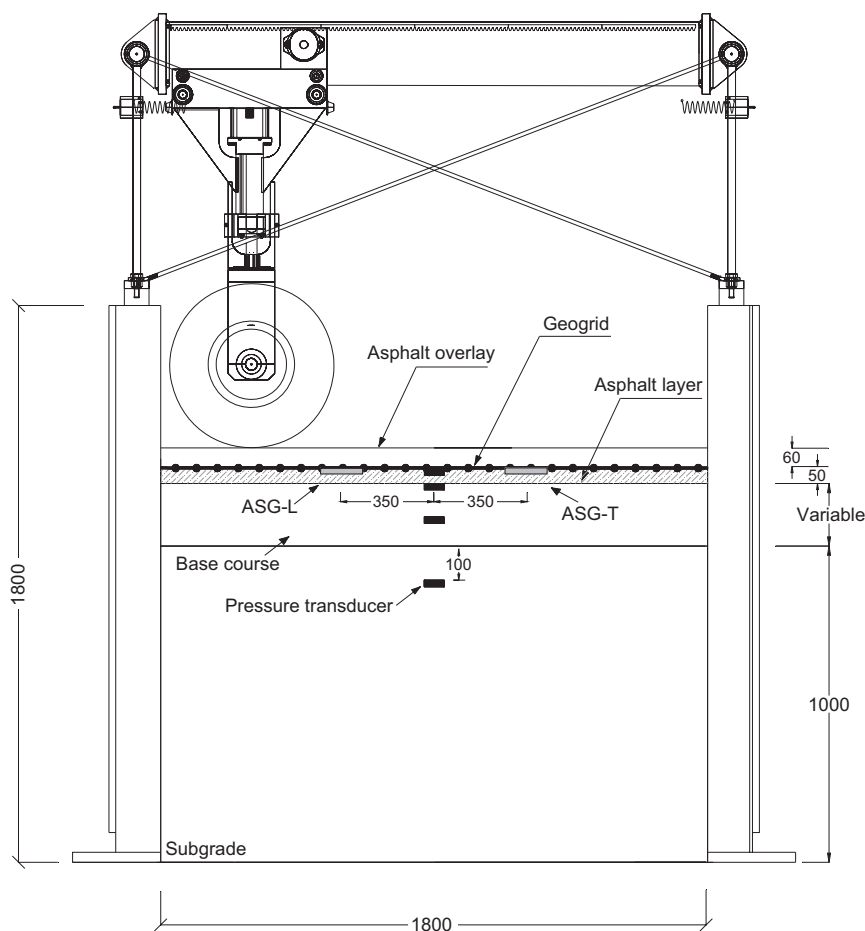


Figure 4. Cross-section view of the pavement layers showing location of the instrumentation devices. Note: dimensions are in mm

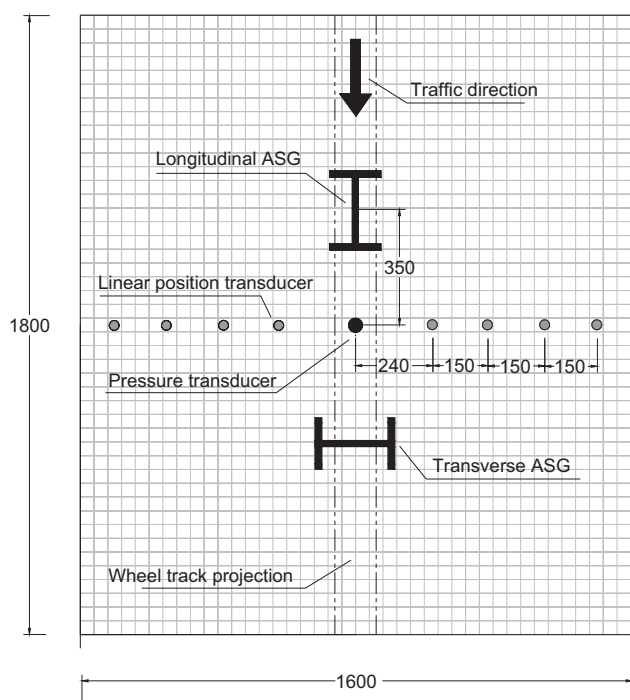


Figure 5. Plan view of the test section showing the locations of the instrumentation devices. Note: distances are in mm

the test section showing the location of the LPTs, ASGs and pressure transducers. Additional measurements of permanent displacements in the wheel load area were conducted using a transverse surface profile. Measurements were taken after 1, 10, 100, 500, 1000, 2500 and 5000 passes, and at intervals of 10 000 wheel passes thereafter. Additional details about the characteristics of the instrumentation used in this study are provided at Correia (2014).

Table 2 provides an overview of the scope of the testing programme. It includes a total of three pavement models (tests 1, 2 and 3), conducted using two stages of tests in each model (stages A and B). In the first stage of tests 1 and 2, identical control sections were loaded until reaching a total of  $10^5$  cycles. The control sections tested as part of this stage (sections 1A and 2A) involved flexible pavement models composed of a 50 mm-thick HMA layer, a 200 mm-thick aggregate base layer and a 1 m-thick subgrade layer. In the second stage of these tests, the HMA overlay was constructed over the previously loaded asphalt surface in order to simulate the loading conditions in an asphalt rehabilitation project.

Table 2. Scope of the testing programme

Test	Stage	Profile name	Geogrid installation	Base course thickness (mm)	Number of load cycles
1	Control	1A	–	200	$10^5$
	Unreinforced HMA overlay	1B	–		$10^5$
2	Control	2A	–	200	$10^5$
	Geogrid-reinforced HMA overlay	2B	Between old and new asphalt layers		$10^5$
3	Control	3A	–	100	$10^5$
	Geogrid-reinforced HMA overlay	3B	Between old and new asphalt layers		–

Test 1 involved a section constructed without reinforcement (section 1B). Test 2 was constructed using layers of the same characteristics of those in layers of Test 1, but included a geogrid-reinforcement in the HMA overlay (section 2B). In both tests, the newly placed HMA overlay was loaded until reaching  $10^5$  cycles. Test 3 was conducted using the same materials and stages as those in test 2, but involved a base course of reduced thickness (100 mm). This configuration was adopted in order to simulate a comparatively less rigid reinforced pavement structure.

Table 3 presents the most relevant properties of the asphalt concrete layers used in each pavement section. These characteristics include the layers thickness ( $t$ ), maximum theoretical specific gravity ( $G_{max}$ ), air void contents (AV), indirect tensile strength (IDT) and resilient modulus ( $M_r$ ). The asphalt concrete layers in all sections and stages presented a comparatively high air voids content, which was attributed to the relatively low compaction effort used in this study.

### 3. RESULTS

#### 3.1. Evaluation of rutting depth

Accumulation of permanent vertical deformations in one or more layers within a pavement system leads to the development of rutting depth. Rutting severely impacts the pavement serviceability, having a significant effect on the cost and schedules of pavement maintenance. In this study, the development of permanent displacements on the pavement surface was measured during the first and second stages of tests. Rutting depth measurements were also used to define the termination of the tests (failure was set as 25 mm rutting). Permanent (plastic) displacements were obtained by subtracting resilient (elastic) displacements from total vertical displacements. Figure 6 shows the development of cumulative plastic displacements obtained during the first stage of tests 1A, 2A and 3A (before placement of HMA overlay). The results on rutting depths obtained for the two identical control sections 1A and 2A show very good repeatability, including essentially the same rut depths at the wheel path (Figure 6a), as well as similar movements alongside the wheel path (Figure 6b). The comparison between the results in the first stage of the tests provided evidence of the consistency of the construction of the pavement models, as well as confidence of the quality control measures adopted in this investigation. The results provide

**Table 3. As-constructed asphalt concrete layers properties**

Property	1A	1B	2A	2B	3A	3B
$t$ (mm)	53.0	61.08	52.1	62.0	52.5	60.0
$G_{max}$ (ASTM D2041M-11)	2.676	2.676	2.677	2.677	2.672	2.672
AV (ASTM D3203M-11)	9.84	10.2	10.4	11.4	9.8	9.0
IDT at 25°C (ASTM D6931-12)	1.09	0.97	1.04	0.88	1.12	0.98
$M_r$ (ASTM D7369-11)	3730	4977	3595	4600	3581	4660

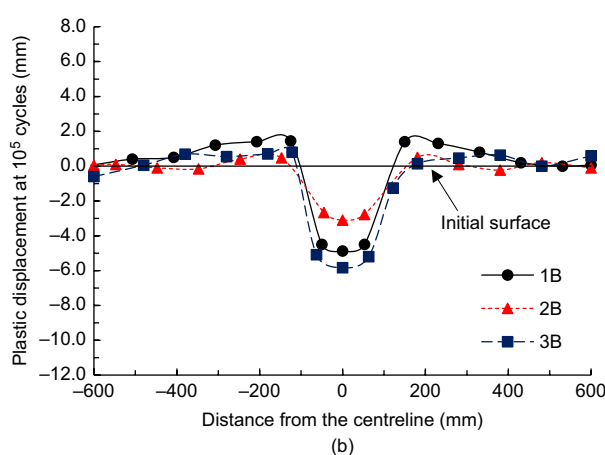
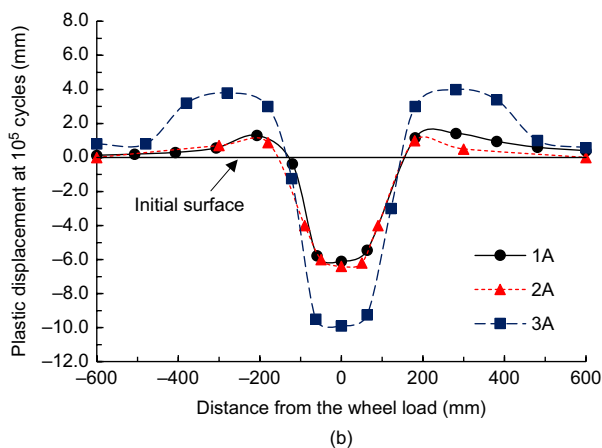
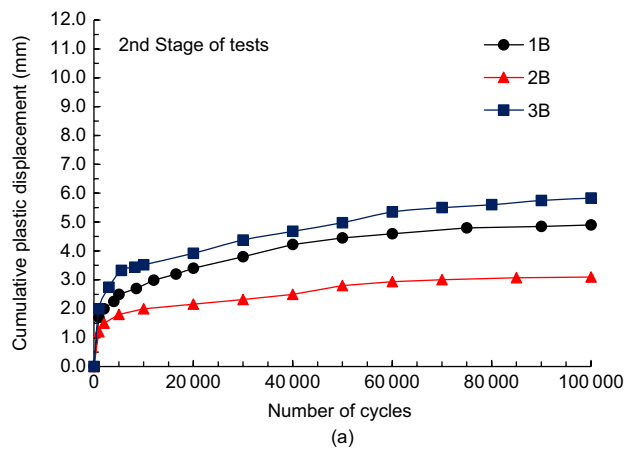
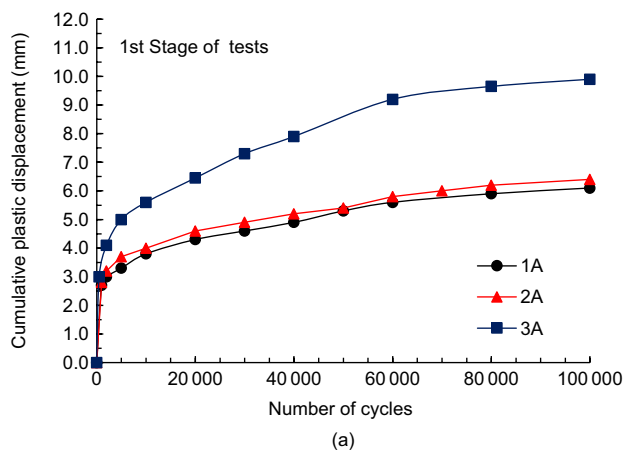


**Figure 6. Results of rutting depth obtained during the first stage of tests: (a) cumulative plastic displacements along the wheel path; (b) rutting profiles after  $10^5$  cycles**

**Figure 7. Results of rutting depth obtained during the second stage of tests (after HMA overlay application): (a) cumulative plastic displacements along the wheel path; (b) rutting profiles after  $10^5$  cycles**

a good basis for the subsequent comparison of the performance of unreinforced and geogrid-reinforced sections. Figure 6 also shows the results obtained in section 3A, constructed with a reduced base course thickness. As expected, the pavement with reduced overall stiffness (3A) shows a significant difference in the cumulative permanent deformation in comparison with the response observed in sections 1A and 2A. In particular, the lateral movement alongside the wheel path on the surface in Section 3A was approximately twice of the values observed in sections 1A and 2A. However, it should be noted that the development of plastic deformations had not stabilised in any of the three sections by the time that the maximum number of cycles was reached. No significant fatigue cracks were noted in control sections.

Figure 7 presents the cumulative permanent displacements obtained during the second stage of the tests. The results indicate that the presence of the HMA overlay led to an increased pavement stiffness and to comparatively smaller rutting in all tests. However, the results also show that the presence of the geogrid led to a substantial decrease in rutting. The benefits of reinforcement inclusion were observed to occur early in the test (Figure 7a), after applying the initial load cycles. In particular, a comparison of the rutting response of sections 1B and 2B reveals that the use of geogrid reinforcement led to 40% decrease in rutting depths after  $10^5$  cycles. Furthermore, a comparison of the response of tests 3B and 1B reveals that the use of asphalt reinforcement led to accumulated rutting that is

similar to the observed in the unreinforced section, which was constructed with a base course layer that is twice as thick as that in the reinforced model.

The results at the end of the tests in Figure 7b indicate that the unreinforced section (1B) shows higher permanent lateral movements next to the wheel path than those obtained when compared with the geogrid-reinforced sections (2B and 3B). It should be noted that all sections were constructed with asphalt surface courses of similar properties and air void contents (Table 3). Overall, it is clear that the presence of the geogrid was effective in reducing permanent deformations of the asphalt layers during cyclic tests (approximately a 40% reduction). The rutting depth results in geogrid-reinforced asphalt overlays obtained in this study were consistent with the trends reported by Brown *et al.* (1985), Laurinavičius and Oginskas (2006), Bühler (2007) and Siriwardane *et al.* (2010).

The rate of vertical displacements has also been utilised to evaluate rutting reduction (Wu *et al.* 2015), which is defined as the changing rate (velocity) of the vertical deformations. Figure 8 shows the rate of permanent displacements, as obtained for tests 1B, 2B and 3B. As shown in the figure, the permanent displacement rate of the section without geogrid (1B) was greater than that of the geogrid-reinforced section (2B). The permanent displacement rate became smaller with increased number of cycles for all tests. However, for section 2B, it became non-significant after 30 000 load cycles, whereas for sections 1B and 3B, the permanent displacement rate remained six times higher and comparatively similar between these sections. The results presented in Figures 7 and 8 suggest that the geogrid reinforcement placed at the bottom of the HMA overlay was effective in reducing rutting depths and permanent lateral movements of the wearing surface, as well as the rate of permanent displacements.

### 3.2. Evaluation of the deflection basins

The area of pavement deflection under and near the load application is known as the ‘deflection basin’. The analysis of the deflection basin (resilient deformation) in

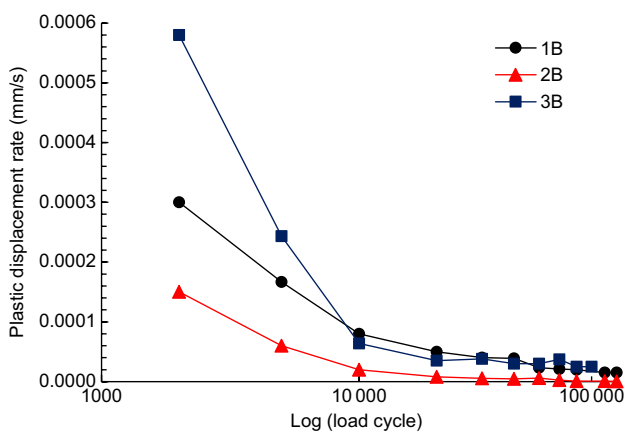


Figure 8. Results of rate of plastic displacements obtained during the second stage of tests, as obtained in tests 1B, 2B and 3B

the asphalt surface provides relevant information for the structural evaluation of new or in-service flexible and rigid pavements (ASTM D4695-03). Figure 9 shows representative results of the deflection basins acquired in the study at the end of  $10^5$  load cycles. Figure 9a shows the deflection basin results for sections 1A, 2A and 3A. As shown in the figure, the deflection basins for the identical control sections 1A and 2A were found to be very similar. The shape of the curves in the vicinity of the wheel load area depends primarily on the stiffness of the asphalt concrete layer, not on the stiffness of subgrade. In the case of section 3A, the characteristics of the deflection basins was primarily affected by the quality of the underlying layers, as shown by the outer edges of the deflection basin. Figure 9b presents the results for the deflection basins obtained at the end of the second stage of the tests 1B, 2B and 3B, showing the general asphalt overlay contribution in reducing resilient deformations. The maximum deflection in section 1B was as high as 0.36 mm. On the other hand, the basin shapes and magnitude of the maximum deflections obtained for the geogrid-reinforced section 2B (max 0.16 mm) were similar to those obtained in section 3B (max 0.22 mm). The basin shapes obtained for these tests represents the significant geogrid contribution to improve pavement structural stiffness. Comparisons of sections 1B and 2B reveals that the use

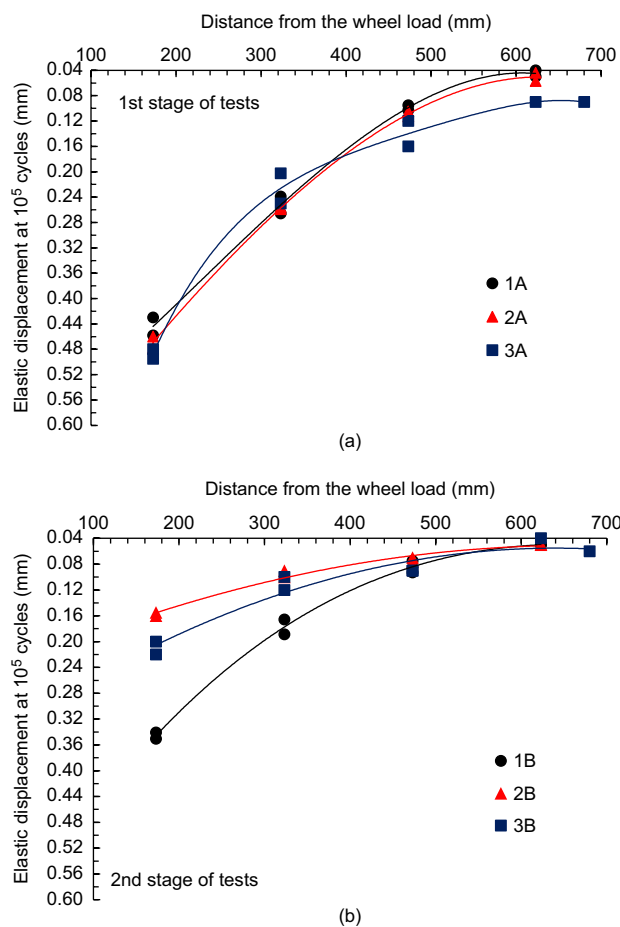


Figure 9. Deflection basins obtained after  $10^5$  load cycles: (a) first stage of tests; (b) second stage of tests (after HMA overly application)

of the geogrid was responsible for a reduction of 55% in the maximum resilient deformations of the asphalt overlay. Overall, the inclusion of geogrid in the asphaltic layer was found to lead to an enhanced overall stiffness in the pavement.

### 3.3. Evaluation of vertical stresses in pavement layers

Instrumentation results also allowed evaluation of the vertical stresses induced by the loading wheel passes (dynamic stress response of the test sections). Specifically, stresses were measured using pressure transducers located beneath the wheel path at the bottom of the asphalt layer, in the middle of the base course and at the top of the subgrade layer, as in Figure 4. The pressure transducer installed at the bottom of the HMA overlay did not produce reliable results in response to traffic loading. This is because transducers were partially damaged during tests, probably due to the proximity (60 mm) of the wheel load contact area.

A typical response of the pressure transducers, as obtained during the second stage of tests, is provided in Figure 10. The stress results show a clear difference between the response of the unreinforced section (1B) and the reinforced section (2B). An average of 32% reduction in vertical stresses at the bottom of the asphalt layer was observed in the geogrid-reinforced section 2B in relation to that in the unreinforced section 1B (Figure 10a). In the middle of the base course, a 30% reduction in vertical stresses was observed in the reinforced section (Figure 10b). Finally, vertical stresses induced at the top of the subgrade resulted in an average 36% reduction due to the presence of reinforcement in the asphalt layer (Figure 10c). The results for reinforced section 3B, in comparison with the results obtained in section 1B, show slightly higher peak values at the bottom of the asphalt layer (Figure 10a). At the middle of the base course, the pressure transducer stopped responding during traffic load, so the results will be further estimated. At the top of the subgrade, the difference in induced stresses between sections 1B and 3B was more pronounced (Figure 10c). Nonetheless, this difference can be attributed to the shorter distance for stress dissipation between the pavement surface and the base layer in Section 3B (100 mm-thick base), when compared with the configuration in section 1B (200 mm-thick base).

Figure 11 presents the vertical stresses measured in the three pavement sections. The results in Figure 11a clearly illustrate the contribution of the polymeric geogrid in reducing the vertical stresses across the base course layers of the pavement sections. These results are consistent with the reductions in vertical stresses on the top of the subgrade, as reported by Siriwardane *et al.* (2010) for the case of fibre-glass geogrids placed within the asphalt layer. Figure 11b illustrates the stress distribution measured on pavement layers of reinforced section 3B. The estimated vertical stress level in the middle of the base course is also shown in the figure. Furthermore, in Figure 11, the stresses in unreinforced section 1B were found to be similar to those in reinforced section 3B (reduced base thickness). The vertical stress results

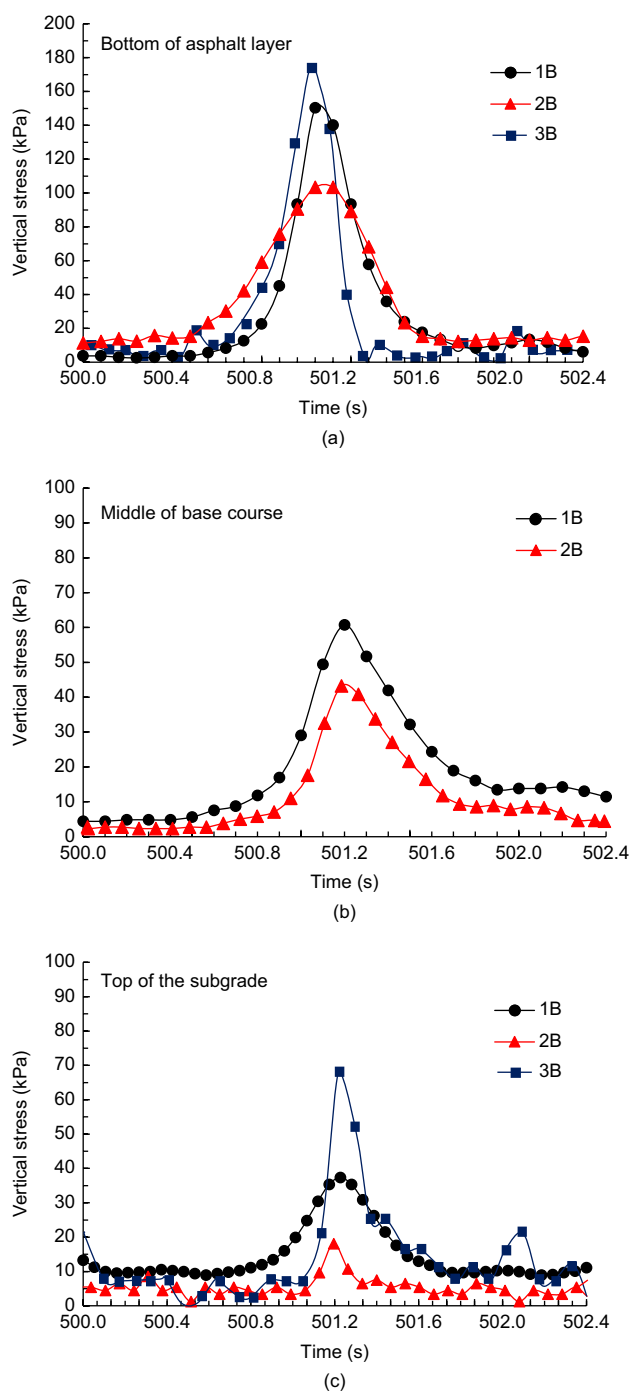


**Figure 10. Typical vertical stress response to cyclic wheel load: (a) bottom of asphalt layer; (b) middle of base course; (c) top of the subgrade**

provide additional evidence that the presence of geogrids in the asphalt layer provides structural benefits to the pavement, leading to reductions in the vertical stresses in the underlying pavement layers.

### 3.4. Evaluation of strains within the asphalt layer

ASGs were installed in the longitudinal and transverse directions of the wheel path (Figure 5) in order to measure load-induced strains in the asphalt layer during traffic loading. Figure 12 illustrates typical elastic strains recorded by the ASG devices in the longitudinal and transverse directions during the tests. Figure 13 shows

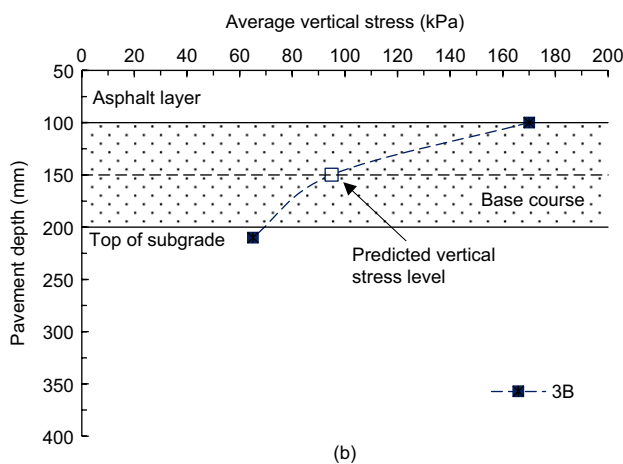
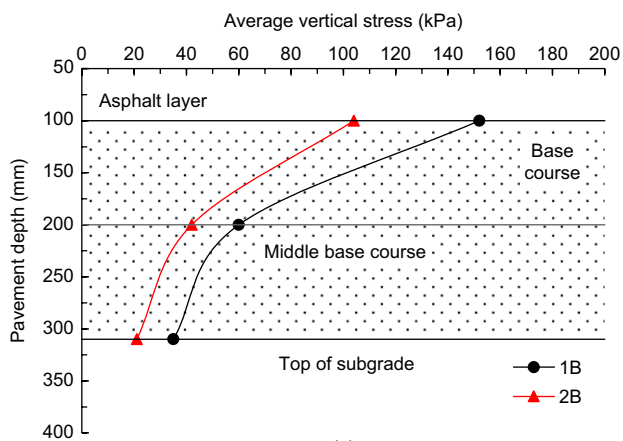


Figure 11. Measured vertical stresses in pavement layers: (a) sections 1B and 2B; (b) section 3B

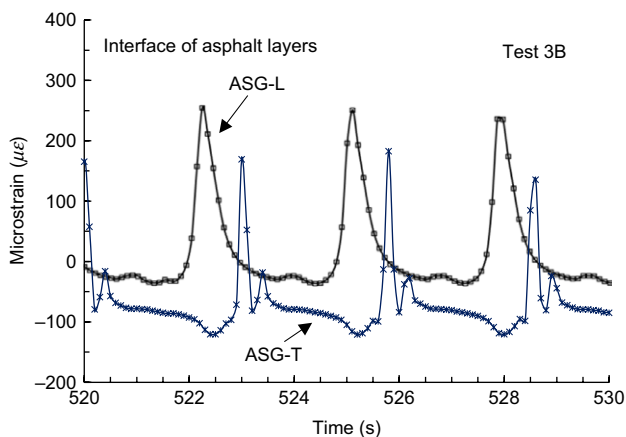


Figure 12. Typical response of ASGs in longitudinal and transverse direction, as obtained in test 3B

the strains measurement, as obtained by the sensors in the transverse direction (ASG-T), for tests 1B, 2B and 3B. The results indicate that the peak transverse tensile strains recorded for section 1B was approximately 200  $\mu\epsilon$ , and the peak strains in section 2B was comparatively smaller (115  $\mu\epsilon$ ). Table 4 summarises the average values of peak tensile strains in the asphalt layer, as measured in both longitudinal (ASG-L) and transverse (ASG-T) directions. Comparison of the tensile strain

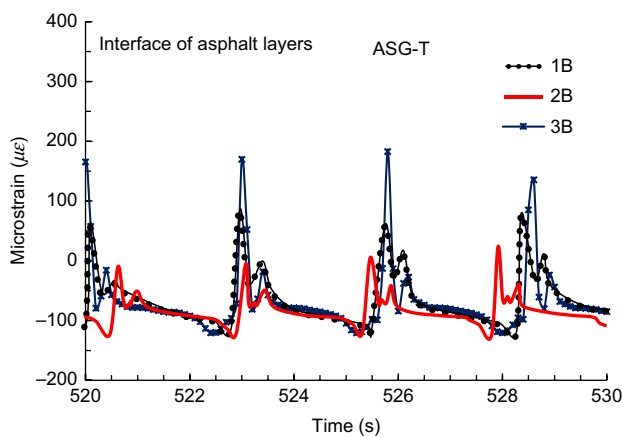


Figure 13. Typical strains at the interface of asphalt layers measured by ASG-T, as obtained in tests 1B, 2B and 3B

Table 4. Average of the peak tensile strains in asphalt concrete layers

Section	Average of the peak tensile strains in asphalt concrete layers	
	Longitudinal strains ( $\mu\epsilon$ ) ASG-L	Transverse strains ( $\mu\epsilon$ ) ASG-T
1B	280	200
2B	125	115
3B	300	330

values reported in Table 4 for sections 1B and 2B highlights the effectiveness of the geogrid to reduce asphalt concrete strain levels (over 40%). Whereas the geogrid-reinforced section 3B exhibited higher transverse strains than the unreinforced section 1B, which was responsible for potential fatigue cracking, the results in the longitudinal direction were found to be comparatively similar. These results illustrate the potential of geogrid reinforcement to reduce asphalt fatigue cracking during the service life of the pavement.

#### 4. CONCLUSIONS

Whereas most previous research on the use of geosynthetics to reinforce asphalt layers has focused on minimising reflective cracking, this study focuses on the use of geosynthetic reinforcements to increase the overall pavement structural capacity. Specifically, this research focused on quantifying the improved permanent and resilient deformations, asphalt concrete strains and vertical stresses expected in pavement layers when using geogrids to reinforce asphalt overlays. An APT facility was developed for this study. The investigation involved large-scale laboratory instrumented pavement models constructed using polyvinyl alcohol geogrids as reinforcement inclusions. Based on the results obtained from this research, the following conclusions can be drawn.

- Analysis of the results obtained in pavement control sections constructed using the same structural layers

and materials were found to provide essentially overall rutting and deflection basin behaviour after wheel cyclic loading. This provides confidence on the quality control measures adopted in the experimental components of this study.

- The improvement in pavement performance that results from the use of geogrids in asphalt overlays could be quantified by comparing the mechanical performance of unreinforced and reinforced sections. In particular, the use of geogrid reinforcement resulted in a 40% decrease in rutting depth and significantly less permanent lateral movements, as well as reductions in the rate of permanent displacements. The use of geogrid reinforcement also resulted in reductions in the asphalt concrete strain levels that were as high as 40%. In addition, resilient displacement levels were reduced up to 55%. Finally, over 30% reduction in vertical stress levels in pavement layers was also attributed to the geogrid inclusion within the asphalt overlays.
- The performance of a pavement section including a geogrid-reinforced asphalt overlay and a reduced base course thickness was found to be comparable to that of a pavement section including an unreinforced asphalt overlay and a thicker base course (twice as thick in this particular study). Specifically, similar behavior was observed in terms of permanent and resilient displacements. Vertical stresses registered in pavement layers and asphalt concrete strain levels in the longitudinal direction were also found to be similar.

Overall, the experimental results generated as part of this study illustrate the improved mechanical performance that resulted from the use of geogrids in asphalt overlays in terms of rutting depths, deflection basins, asphalt concrete strains and vertical stresses. In addition to the more common use of geosynthetics to minimise reflective cracking, geogrid reinforcements within asphalt overlays were found to be effective in enhancing the overall stiffness of the pavement. Consequently, the inclusion of geogrid in the asphalt overlay was recognised as acting as a reinforcement element, providing enhanced structural capacity to flexible pavement structures.

## ACKNOWLEDGEMENTS

The authors are grateful to the late B. Bueno for his contributions to this study. Support provided by the National Council for Scientific and Technological Development (CNPq) and by Huesker Geosynthetics is also gratefully acknowledged.

## NOTATION

Basic SI units are given in parentheses.

AV	air void contents (dimensionless)
$G_{\max}$	asphalt concrete maximum theoretical specific gravity (dimensionless)

$M_r$	resilient modulus (Pa)
$t$	thickness (m)

## REFERENCES

- AASHTO (1999) M-145 *Classification of Soils and Soil-Aggregate Mixtures for Highway Construction Purposes*. AASHTO Standard Specifications for Transportation Materials, Part II, Washington, DC, USA. See <http://www.techstreet.com/products/1320718>.
- ASTM D2041M-11 *Standard Test Method for Theoretical Maximum Specific Gravity and Density of Bituminous Paving Mixtures*. ASTM International, West Conshohocken, PA, USA.
- ASTM D2487-11 *Standard Practice for Classification of Soils for Engineering Purposes (Unified Soil Classification System)*. ASTM International, West Conshohocken, PA, USA.
- ASTM D3203M-11 *Standard Test Method for Percent Air Voids in Compacted Dense and Open Bituminous Paving Mixtures*. ASTM International, West Conshohocken, PA, USA.
- ASTM D4695-03 *Standard Guide for General Pavement Deflection Measurements*. ASTM International, West Conshohocken, PA, USA.
- ASTM D6637-11 *Standard Test Method for Determining Tensile Properties of Geogrids by the Single or Multi-Rib Tensile Method*. ASTM International, West Conshohocken, PA, USA.
- ASTM D6931-12 *Standard Test Method for Indirect Tensile (IDT) Strength of Bituminous Mixtures*. ASTM International, West Conshohocken, PA, USA.
- ASTM D7369-11 *Standard Test Method for Determining the Resilient Modulus of Bituminous Mixtures by Indirect Tension Test*. ASTM International, West Conshohocken, PA, USA.
- Austin, R. A. & Gilchrist, A. J. T. (1996). Enhanced performance of asphalt pavements using geocomposites. *Geotextiles and Geomembranes*, **14**, No. 3-4, 175-186.
- Brown, S. F., Hughis, D. A. B. & Brodrick, B. V. (1985). *Polymer Grid Reinforcement*, Thomas Telford Limited, London, UK, pp. 158-165.
- Bühler, A. (2007). *Study the Effect of Grid Reinforcement in Pavement Restoration*, PhD dissertation, ITA, Sao Jose dos Campos, SP, Brazil. (in Portuguese).
- Canestrari, F., Belogi, L., Ferrotti, G. & Graziani, A. (2015). Shear and flexural characterization of grid-reinforced asphalt pavements and relation with field distress evolution. *Materials and Structures*, **48**, No. 4, 959-975.
- Correia, N. S. (2014). *Performance of Flexible Pavements Enhanced with Geogrid-Reinforced Asphalt Overlays*, PhD dissertation, University of Sao Paulo, Sao Paulo, Brazil, 201p.
- DNER P00/043 (2006). *National Department of Highways of Sao Paulo State. Technical Specification – Anti-reflective Cracking System with Geosynthetics*, Sao Paulo, Brazil (in Portuguese).
- Fallah, S. & Khodaii, A. (2015). Reinforcing overlay to reduce reflection cracking; an experimental investigation. *Geotextiles and Geomembranes*, **43**, No. 3, 216-227.
- Ferrotti, G., Canestrari, F., Pasquini, E. & Virgili, A. (2012). Experimental evaluation of the influence of surface coating on fiberglass geogrid performance in asphalt pavements. *Geotextiles and Geomembranes*, **34**, 11-18.
- FHWA (Federal Highway Administration) and NAPA (National Asphalt Pavement Association) (2001). *HMA Pavement Mix Type Selection Guide*. Information series 128, Federal Highway Administration, U.S. Department of Transportation. National Asphalt Pavement Association, Washington DC, USA.
- Gonzalez-Torre, I., Calzada-Perez, M. A., Vega-Zamanillo, A. & Castro-Fresno, D. (2015). Experimental study of the behavior of different geosynthetics as anti-reflective cracking systems using a combined-load fatigue test. *Geotextiles and Geomembranes*, **43**, No. 4, 345-350.
- Graziani, A., Pasquini, E., Ferrotti, G., Virgili, A. & Canestrari, F. (2014). Structural response of grid-reinforced bituminous pavements. *Materials and Structures*, **47**, No. 8, 1391-1408.

- Holtz, R. D., Christopher, B. R. & Berg, R. R. (1998). *Geosynthetic Design and Construction Guidelines*, Federal Highway Administration, Washington, DC, USA, FHWA-HI-98-038.
- Khodaii, A., Fallah, S. & Moghadas Nejad, F. (2009). Effects of geosynthetics on reduction of reflection cracking in asphalt overlays. *Geotextiles and Geomembranes*, **27**, No. 1, 1–8.
- Laurinavičius, A. & Oginskas, R. (2006). Experimental research on the development of rutting in asphalt concrete pavements reinforced with geosynthetic materials. *Journal of Civil Engineering and Management*, **12**, No. 4, 311–317.
- Lytton, R. L. (1989). Use of geotextiles for reinforcement and strain relief in asphalt concrete. *Geotextiles and Geomembranes*, **8**, No. 3, 217–237.
- Mounes, S. M., Karim, M. R., Khodaii, A. & Almasi, M. H. (2015). Evaluation of permanent deformation of geogrid reinforced asphalt concrete using dynamic creep test. *Geotextiles and Geomembranes*, **44**, No. 1, 109–116.
- Pasquini, E. & Bocci, M. (2014). Laboratory characterization of optimized geocomposites for asphalt pavement reinforcement. *Geosynthetics International*, **21**, No. 1, 24–36.
- Perkins, S. W. (1999). Mechanical response of geosynthetic-reinforced flexible pavements. *Geosynthetics International*, **6**, No. 5, 347–382.
- Perkins, S. W. & Ismeik, M. (1997). A synthesis and evaluation of geosynthetic-reinforced base course layers in flexible pavements: part I experimental work. *Geosynthetics International*, **4**, No. 6, 549–604.
- Prieto, J. N., Gallego, J. & Perez, I. (2007). Application of the wheel reflective cracking test for assessing geosynthetics in anti-reflection pavement cracking systems. *Geosynthetics International*, **14**, No. 5, 287–297.
- Siriwardane, H., Gondle, R. & Bora, K. (2010). Analysis of flexible pavements reinforced with geogrids. *Geotechnical and Geological Engineering*, **28**, No. 3, 287–297.
- Solaimanian, M. (2013). *Evaluating Resistance of Hot Mix Asphalt to Reflective Cracking Using Geocomposites*, Transportation Research Building, Report No. PSU-2008-04. The Pennsylvania State University, City of State College, PA, USA 16802-4710, 36p.
- Tang, X., Soffels, S. M. & Palomino, A. M. (2015) Mechanistic-empirical approach to characterizing permanent deformation of reinforced soft soil subgrade. *Geotextiles and Geomembranes*, 1–13. <http://dx.doi.org/10.1016/j.geotextmem.2015.06.004>.
- Timm, D., Priest, A. & Mcewen, T. V. (2004). *Design and Instrumentation of the Structural Pavement Experiment at the Ncat Test Track*, National Center for Asphalt Technology-NCAT, Report 04-01, Auburn University, Auburn, AL, USA.
- USACOE (United States Army Corp of Engineers) (2003). *Use of Geogrids in Pavement Construction*, ETL 1110-1-189. United States Army Corp of Engineers, Washington, DC, USA.
- Virgili, A., Canestrari, F., Grilli, A. & Santagata, F. A. (2009). Repeated load test on bituminous systems reinforced by geosynthetics. *Geotextiles and Geomembranes*, **27**, No. 3, 187–195.
- Wu, H., Huang, B., Shu, X. & Zhao, S. (2015). Evaluation of geogrid reinforcement effects on unbound granular pavement base courses using loaded wheel tester. *Geotextiles and Geomembranes*, **43**, No. 5, 462–469.
- Yu, B., Lu, Q. & Yang, J. (2013). Evaluation of anti-reflective cracking measures by laboratory test. *International Journal of Pavement Engineering*, **14**, No. 6, 553–560.
- Zamora-Barraza, D., Calzada-Perez, M., Castro-Fresno, D. & Vega Zamanillo, A. (2010). New procedure for measuring adherence between a geosynthetic material and a bituminous mixture. *Geotextiles and Geomembranes*, **28**, No. 5, 483–489.
- Zornberg, J. G. & Gupta, R. (2010). Geosynthetics in pavements: North American contributions. Theme speaker lecture. *Proceedings of the 9th International Conference on Geosynthetics*, Brazilian Chapter of the International Geosynthetics Society, Guarujá, SP, Brazil, Vol. 1, pp. 379–400.

**The Editor welcomes discussion on all papers published in *Geosynthetics International*. Please email your contribution to [discussion@geosynthetics-international.com](mailto:discussion@geosynthetics-international.com)**